JOURNAL OF SOLID STATE CHEMISTRY 92, 352–361 (1991)

Synthesis, Structure, and Physical Properties of the New Layered Ternary Telluride $TaPtTe_5$

ARTHUR MAR AND JAMES A. IBERS

Department of Chemistry and Science and Technology Center for Superconductivity, Northwestern University, Evanston, Illinois 60208

Received October 30, 1990

The new ternary telluride $TaPtTe_5$ has been prepared. It is a metallic, layered material whose structure has been determined by single-crystal X-ray diffraction methods. $TaPtTe_5$ is isostructural with $NbNiTe_5$ and $TaNiTe_5$. It crystallizes in space group D_{2h}^{17}-*Cmcm* of the orthorhombic system with four formula units in a cell of dimensions $a = 3.729(4)$, $b = 13.231(11)$, $c = 15.452(10)$ Å. The layers consist of bicapped trigonal prismatic Ta atoms and octahedral Pt atoms coordinated by Te atoms. $TaPtTe_5$ displays good metallic conductivity along the a axis ($\sigma_{298} = 9.7 \times 10^4\ \Omega^{-1}\ cm^{-1}$) and is Pauli-paramagnetic ($\chi = 2.1 \times 10^{-4}$ emu mol^{-1}). The electrical and magnetic properties of $TaPtTe_5$ are compared with those of $NbNiTe_5$ and $TaNiTe_5$, as well as with the related compound $NbPdTe_5$. $NbPdTe_5$ contains layers identical with those of the present series of compounds but stacked differently; it is a relatively poor metallic conductor.

Introduction

Many binary and ternary chalcogenides of Nb and Ta adopt low-dimensional or layered structures that can give rise to unusual physical properties (e.g., superconductivity (*1–4*), charge density waves (*5–8*)) as well as an extensive intercalation chemistry (*9–11*). Although many ternary sulfides and selenides are now known, relatively few tellurides have been synthesized. Our efforts to prepare new ternary transition-metal tellurides of the formulation $M_xM'_yTe_z$ (M = Nb, Ta and M' = Ni, Pd, Pt) are motivated by the desire to extend the chemistry of the ternary sulfides and selenides previously developed in this laboratory. Our synthetic strategy has been guided by a knowledge of preferred coordination geometries of the transition metals and how the coordination polyhedra can be linked (*12*).

The layered compounds $NbNiTe_5$ (*13*), $NbPdTe_5$ (*14*), and $TaNiTe_5$ (*15*) were recently described. They possess a common layer composed of two different chains of metal-centered polyhedra joined in an alternating fashion: Nb or Ta bicapped trigonal prisms sharing their triangular faces, and Ni or Pd edge-sharing octahedra. Depending on the relative positions of the metal chains in adjacent layers, we describe the stacking to be "eclipsed" in $NbNiTe_5$ and $TaNiTe_5$ but "staggered" in $NbPdTe_5$, as shown in Fig. 1. Both $NbNiTe_5$ and $TaNiTe_5$ display high metallic conductivities along the direction of their metal chains (along the a axis), while $NbPdTe_5$ displays relatively poor metallic conductivity along the direction of its metal chains (along the b axis). The magnetic susceptibilities of $NbNiTe_5$ and $TaNiTe_5$ were reported to obey the Curie–Weiss law; this behavior is considered unusual for metals.

0022-4596/91 $3.00

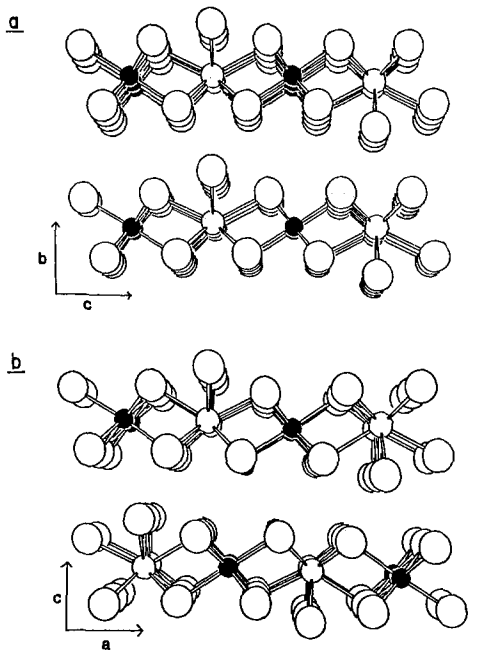

FIG. 1. (a) View of $NbNiTe_5$ or $TaNiTe_5$ down the *a* axis showing the eclipsed stacking of the layers. Small open circles are Nb or Ta atoms, small solid circles are Ni atoms, and large open circles are Te atoms. (b) View of $NbPdTe_5$ down the *b* axis showing the staggered stacking of the layers. Small open circles are Nb atoms, small solid circles are Pd atoms, and large open circles are Te atoms.

The magnetic properties of $NbPdTe_5$ have not been previously measured.

The synthesis, structure, and electrical conductivity of another member of this series of compounds, $TaPtTe_5$, is reported here. In addition, the magnetic properties of the entire series have now been investigated. An attempt is made to relate the electrical and magnetic properties of this series of compounds to their structural features and metal substitutions.

Experimental

Synthesis of $TaPtTe_5$. Powders of the elements in an atomic ratio of Ta : Pt : Te = 1 : 1 : 5 (Ta, 45 mg, 0.25 mmol, 99.98%; Pt, 48 mg, 0.25 mmol, 99.99%; Te, 157 mg, 1.23 mmol, 99.999%; all from AESAR) were ground together. The reactants were loaded into a silica tube (10 cm length, 10 mm ID) that was then evacuated to $\sim 5 \times 10^{-5}$ Torr and sealed off at 5 cm. The tube was heated in a furnace for 4 days at 1000°C. Small shiny black needle-shaped crystals were obtained. These contained Ta, Pt, and Te, as determined by a microprobe analysis with an EDAX equipped Hitachi S570 scanning electron microscope. Subsequently it was found that better crystals could be obtained by use of an excess of Te (Ta : Pt : Te = 1 : 1 : 10) and a heating regime of 500°C for 1 day, 800°C for 1 day, 1000°C for 4 days, and then cooling to room temperature for 1 day. Impurities of the binaries ($TaTe_2$, $TaTe_4$, $PtTe_2$) were always formed, as determined from X-ray powder diffraction patterns obtained on an Enraf–Nonius FR522 Guinier camera. The use of I_2 as a vapor transport agent was unsuccessful; even small amounts of I_2 lead to the preferential formation of $TaTe_4$.

We have attempted to synthesize the analogue, $NbPtTe_5$, but to no avail. Use of a variety of heating conditions (300 to 1200°C), of different loading compositions of reactants, of transport agents ($TeCl_4$, I_2), and of pellet pressing, have all failed to produce a ternary compound in the Nb/Pt/Te system. Only the binaries $NbTe_4$, $NbTe_2$, and $PtTe_2$ were formed.

Electrical conductivity. Single crystals of $TaPtTe_5$ averaging 1 mm in length and 5×10^{-4} mm^2 in cross-sectional area were mounted with Ag paint on Al wires extended by graphite fibers. Because $TaTe_4$ is a common impurity whose color and needle-shaped habit are easily confused with those of $TaPtTe_5$, the integrity of the mounted crystals was first checked by EDAX measurements. The electrical conductivity along the needle axis *a* of $TaPtTe_5$ was then measured by a four-probe ac (27 Hz) phase-locked technique as described previously

TABLE I

CRYSTAL DATA AND INTENSITY COLLECTION FOR $TaPtTe_5$

Formula	$TaPtTe_5$
Formula mass (amu)	1014.04
Space group	D_{2h}^{17}-*Cmcm*
a (Å)	3.729(4)[a]
b (Å)	13.231(11)
c (Å)	15.452(10)
V (Å^3)	762.4
Z	4
ρ_c (g cm^{-3})	8.83
T of data collection (K)[b]	111
Radiation	Graphite monochromated Mo$K\alpha$ ($\lambda(K\alpha_1)$ = 0.7093 Å)
Crystal shape	Needle 0.37 × 0.02 × 0.01 mm bounded by {100}, {010}, {001}
Crystal volume (mm^3)	7.36 10^{-5}
Linear abs. coeff. (cm^{-1})	514
Transmission factors[c]	0.314-0.604
Detector aperture (mm)	Horizontal, 6.0; vertical, 6.0; 32 cm from crystal
Takeoff angle (degrees)	2.5
Scan type	ω
Scan speed (degrees min^{-1})	1.0 in ω
Scan range (degrees)	−1.1 to +1.1 in ω
λ^{-1} sin θ, limits (Å^{-1})	0.031–0.906 $2.5° \leq 2\theta(\text{Mo}K\alpha_1) \leq 80°$
Background counts	20 sec at each end of scan with rescan option[d]
Data collected	$+h, +k, +l$
p factor	0.04
No. of data collected	1398
No. of unique data, including $F_o^2 < 0$	1398
No. of unique data, with $F_o^2 > 3\sigma(F_o^2)$	679
No. of variables	24
$R(F^2)$	0.159
$R_w(F^2)$	0.183
R (on *F* for $F_o^2 > 3\sigma(F_o^2)$)	0.070
Error in observation of unit weight (e^2)	1.39

[a] Obtained from a refinement constrained so that $\alpha = \beta = \gamma = 90°$.

[b] The low-temperature system is based on a design by Huffman (*37*).

[c] The analytical method as employed in the Northwestern absorption program, AGNOST, was used for the absorption correction (*38*).

[d] The diffractometer was operated using the Vanderbilt disk-oriented system (*39*).

(*16*). Samples were cooled at a rate of approximately 1°C min^{-1} by use of a flow of cold helium gas. The greatest uncertainty in these measurements arises from difficulties in measuring the cross-sectional area of the crystals, propagating as an uncertainty in the conductivity values of $(\Delta\sigma)/\sigma = \pm 0.2$.

Magnetic susceptibility. Magnetic data

for $NbNiTe_5$ and $TaNiTe_5$ (but not $NbPdTe_5$) have been reported previously (*13, 15*), but the purity of the samples used was not assessed. $NbNiTe_5$, $NbPdTe_5$, and $TaNiTe_5$ were prepared as described previously (*13–15*), and $TaPtTe_5$ was prepared as described above. In all cases, only single crystals or aggregates of single crystals were manually selected. Several crystals were chosen at random from each sample and their compositions confirmed by EDAX measurements. Except for $TaPtTe_5$, the crystals were then ground to fine powders that were further identified by X-ray powder diffraction. We estimate the purity of all four samples to be >95%.

Variable-temperature magnetic susceptibility measurements were made from 4.5 to 300 K at a field strength of 5 kG with a Quantum Design SQUID magnetometer. Sample weights were 3.6, 33.4, 29.2, and 25.7 mg for $NbNiTe_5$, $NbPdTe_5$, $TaNiTe_5$, and $TaPtTe_5$, respectively. The magnetic moment data were corrected for background contributions from the sample holder over the entire temperature range. At 4.5 K, the magnetizations of all samples were linearly proportional to the applied field strengths from 5 to 10 kG. The raw susceptibility data were corrected for ion-core diamagnetic contributions for Nb^{5+}, Ta^{5+}, Ni^{2+} Pd^{4+} Pt^{4+}, and Te^{2-} (*17*) to obtain the molar paramagnetic susceptibilities of the compounds.

Structure determination of $TaPtTe_5$. Analysis of oscillation and Weissenberg photographs of $TaPtTe_5$ revealed Laue symmetry *mmm* and gave preliminary cell parameters. The systematic extinctions (*hkl*, $h + k = 2n + 1$; *h*0*l*, $l = 2n + 1$) are consistent with the orthorhombic space groups D_{2h}^{17}-*Cmcm*, C_{2v}^{12}-$Cmc2_1$, and C_{2v}^{16}-*C*2*cm*. The final cell parameters were determined from least-squares analysis of the setting angles of 12 reflections in the range $28° < 2\theta(\text{Mo}K\alpha_1) < 34°$ automatically centered on a Picker FACS-1 diffractometer. Diffraction data were collected at −162°C. Six standard reflections monitored at intervals of every 100 reflections showed no significant change during the course of data collection. Crystal data and further details of the data collection are given in Table I.

Calculations were carried out on a Harris 1000 computer with programs standard in this laboratory (*18*). Conventional atomic scattering factors and anomalous dispersion corrections were used (*19*). The intensity data were processed and corrected for absorption effects. From the similarity of cell parameters, we assumed that $TaPtTe_5$ is isostructural with $TaNiTe_5$, and so the space group *Cmcm* was chosen and the initial positions for all atoms in $TaPtTe_5$ were taken from those of $TaNiTe_5$. The structure was refined by least-squares methods, in which the function minimized was $\Sigma w(F_o^2\text{-}F_c^2)^2$. The final cycle of refinement on F_o^2 included anisotropic thermal parameters and resulted in a value of $R(F_o^2)$ of 0.159. The value for the conventional R index (on F for $F_o^2 > 3\sigma(F_o^2)$) is 0.070. The final difference electron density map shows no features with a height greater than 1.4% that of a Pt atom. No unusual trends were observed from an analysis of F_o^2 versus F_c^2 as a function of F_o^2, λ^{-1} sin θ, and Miller indices. Final values of the atomic parameters and equivalent isotropic thermal parameters are given in Table II. These thermal parameters are unexcep-

TABLE II

POSITIONAL PARAMETERS AND EQUIVALENT ISOTROPIC THERMAL PARAMETERS FOR $TaPtTe_5$

Atom	Wyckoff position	x	y	z	B_{eq} (Å^2)
Ta	4*c*	1/2	−0.01245(14)	1/4	0.75(3)
Pt	4*a*	0	0	0	0.85(3)
Te(1)	8*f*	0	0.10104(15)	0.14796(10)	0.85(4)
Te(2)	8*f*	1/2	0.11081(15)	0.58024(10)	0.86(4)
Te(3)	4*c*	0	0.17277(21)	3/4	0.90(6)

Note. $B_{eq} = (8\pi^2/3) \sum_i \sum_j U_{ij} a_i^* a_j^* \mathbf{a}_i \cdot \mathbf{a}_j$.

tional and support an ordered structure with the stoichiometry $TaPtTe_5$. Final anisotropic thermal parameters are given in Table III.[1] Generally, thermal vibration is contracted along the *c* direction. This may be an artifact arising from the absorption correction and its sensitivity to small crystal imperfections. Structure amplitudes are given in Table IV.[1]

Results

Description of the structure. Selected interatomic distances and angles for $TaPtTe_5$ are given in Table V. A view down the *a* axis is given in Fig. 2, which shows the eclipsed stacking of the layers. Figure 3 shows that an individual layer is composed of chains of face-sharing Ta bicapped trigonal prisms and edge-sharing Pt octahedra. This compound is isostructural with $NbNiTe_5$ and $TaNiTe_5$, and a detailed description of this structural type has been given previously (*13, 15*). $NbPdTe_5$ is of a different structural type with staggered, rather than eclipsed, stacking of the layers. Table VI compares important interatomic distances in $NbNiTe_5$, $TaNiTe_5$, $NbPdTe_5$, and $TaPtTe_5$. While the metrical details of $NbNiTe_5$ and $TaNiTe_5$ are practically identical, there are small but noticeable expansions of bond distances in $NbPdTe_5$ and $TaPtTe_5$. The substitution of Ta for Nb introduces no significant structural change because of their similarity in size (*20*), but the substitution of the larger Pd or Pt atom for Ni results in the expected expansions.

TABLE V

SELECTED INTERATOMIC DISTANCES (Å) AND ANGLES (DEGREES) FOR $TaPtTe_5$

Ta–2Te(3)	2.824(3)	Te(3)–Ta–Te(3)	82.64(12)
Ta–4Te(1)	2.867(2)	Te(3)–Ta–2Te(2)	70.50(5)
Ta–2Te(2)	2.928(2)	Te(3)–Ta–2Te(1)	87.93(8)
Ta–2Ta	3.729(4)	Te(2)–Ta–Te(2)	127.23(11)
Ta–4Pt	4.293(2)	Te(1)–Ta–2Te(2)	74.93(6)
		Te(1)–Ta–2Te(1)	66.74(8)
Pt–2Te(1)	2.648(2)	Te(1)–Ta–2Te(1)	81.15(9)
Pt–4Te(2)	2.677(2)		
Pt–2Pt	3.729(4)	Te(1)–Pt–4Te(2)	97.09(6)
		Te(2)–Pt–2Te(2)	91.68(9)
Te(1)–Te(1)	3.153(4)		
Te(1)–2Te(2)	3.525(3)		
Te(1)–2Te(1)	3.729(4)		
Te(1)–2Te(3)	3.863(4)		
Te(1)–2Te(2)	3.991(3)		
Te(2)–2Te(3)	3.321(2)		
Te(2)–2Te(2)	3.729(4)		
Te(2)–Te(2)	3.840(4)		
Te(3)–2Te(3)	3.729(4)		

The bicapped trigonal prismatic coordination around the Ta atom in $TaPtTe_5$ is distorted such that one side of the triangular faces is relatively short (3.153(4) Å) compared to the remaining two sides (3.836(4) Å). An even shorter distance is found in other tellurides exhibiting a bicapped trigonal prismatic geometry, such as $K_4Hf_3Te_{17}$ (2.804(5)–2.933(4) Å) (*21*) and $Cu_{1.85}Zr_2Te_6$ (2.735(2) Å) (*22*). In $HfTe_5$, a full Te–Te bond is found (2.763(4) Å) (*23*). Such Te–Te distances, which are shorter than the ionic Te^{2-}–Te^{2-} separation (4.2 Å) (*20*), are prevalent in the metal tellurides (*24*).

Electrical conductivity. Plots of the electrical conductivity along the needle axis *a* as a function of temperature are shown in Fig. 4 for $TaPtTe_5$, as well as for $TaNiTe_5$ and $NbNiTe_5$. In this set of isostructural compounds, the electrical conductivity increases in the order $NbNiTe_5 < TaNiTe_5 < TaPtTe_5$. In contrast, the conductivity of

[1] See NAPS document No. 04851 for 8 pages of supplementary materials. Order from ASIS/NAPS. Microfiche Publications, P.O. Box 3513, Grand Central Station, New York, NY 10163-3513. Remit in advance $4.00 for microfiche copy or $7.75 for photocopy. All orders must be prepaid. Institutions and Organizations may order by purchase order. However, there is a billing and handling charge for this service of $15. Foreign orders add $4.50 for postage and handling, $1.50 for postage of any microfiche orders.

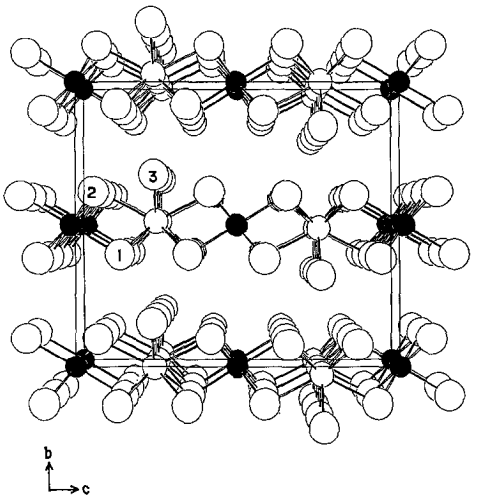

FIG. 2. View of $TaPtTe_5$ down the *a* axis showing the labeling scheme. Here and in Fig. 3 small open circles are Ta atoms, small solid circles are Pt atoms, and large open circles are Te atoms.

$NbPdTe_5$ along its needle axis *b* (Fig. 4) is more than an order of magnitude lower ($\sigma_{295} = 1.3 \times 10^3$; $\sigma_{10} = 5 \times 10^3\ \Omega^{-1}\ cm^{-1}$) (*14*). Prior to the present synthesis of $TaPtTe_5$, it was unclear whether this dramatic difference in conductivity was the result of the metal substitution (Ni, Pd) or the different layer stacking ($NbNiTe_5$, $TaNiTe_5$, eclipsed stacking; $NbPdTe_5$, staggered stacking). The high conductivity of $TaPtTe_5$ (eclipsed stacking) suggests that it is the way the layers are stacked and not the metal (Ni, Pd, Pt) that is the dominant factor in determining the electrical properties of these compounds.

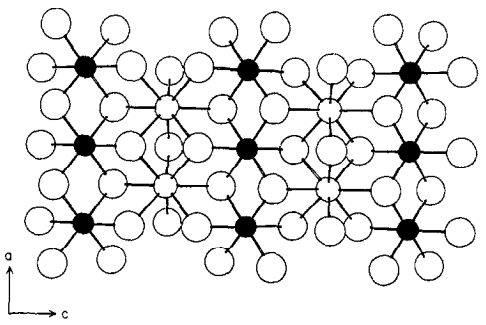

FIG. 3. View of $TaPtTe_5$ down the *b* axis showing an individual layer and the coordination around the Ta and Pt atoms.

The anisotropic conductivity of $NbNiTe_5$ was previously justified by extended Hückel tight-binding calculations (*25*). The metallic conductivity within a layer has been attributed to dispersive bands crossed by the Fermi level. These bands are composed primarily of Te 5*p* orbitals oriented parallel to the chains of metal atoms. We postulate that the conductivity *within* a layer is affected to some degree by weak Te · · · Te interactions across the van der Waals' gap *between* adjacent layers. Inspection of the trend (Fig. 5) in shortest interlayer distances (3.666(2), 3.789(3), 3.812(2), and 3.863(4) Å for $NbPdTe_5$, $NbNiTe_5$, $TaNiTe_5$, and $TaPtTe_5$, respectively) suggests that the conductivity of $NbPdTe_5$ may be diminished because the smaller separation between the layers would introduce more perturbation on the migration of charge within individual layers. A similar explanation has been offered (*26*) to explain differences in conductivity between $Ta_3Pd_3Te_{14}$ (*15*) and $Ta_4Pd_3Te_{16}$ (*26*). At least for the present series of compounds, structural differences rather than metal substitution appear to be responsible for the great contrast in electrical conductivity between $NbPdTe_5$ on one hand, and $NbNiTe_5$, $TaNiTe_5$, and $TaPtTe_5$ on the other hand (Fig. 4). The latter isostructural compounds show some differences in electrical conductivity; these could arise from metal substitution as well as from layer separation.

Magnetic susceptibility. Plots of the molar magnetic susceptibility (corrected for ion-core diamagnetism) as a function of temperature are shown in Fig. 6. $NbPdTe_5$ is paramagnetic with a fairly constant suscep-

TABLE VI

COMPARISON OF IMPORTANT INTERATOMIC DISTANCES (Å) IN $MM'Te_5$ (M = Nb, Ta; M' = Ni, Pd, Pt)

	$NbPdTe_5$	$NbNiTe_5$	$TaNiTe_5$	$TaPtTe_5$
Range of M–Te	2.834(2)–2.947(3)	2.808(3)–2.921(3)	2.804(2)–2.923(2)	2.824(3)–2.928(2)
Range of M'–Te	2.667(2)–2.708(2)	2.557(3)–2.574(2)	2.557(2)–2.575(1)	2.649(3)–2.677(2)
Shortest M–M	3.728(2)	3.656(5)	3.659(2)	3.729(4)
Shortest M'–M'	3.728(2)	3.656(5)	3.659(2)	3.729(4)
Shortest M–M'	4.337(3)	4.200(4)	4.201(3)	4.293(2)
Shortest Te–Te:				
Intralayer	3.242(2)	3.196(4)	3.183(3)	3.153(4)
Interlayer	3.666(2)	3.789(3)	3.812(2)	3.863(4)

tibility (5.2×10^{-4} emu mol^{-1}) that begins to increase slightly below 30 K. The measured susceptibility of $TaPtTe_5$ is actually negative and constant (-1.8×10^{-4} emu mol^{-1}), but when corrected for ion-core diamagnetism, it is small and positive (2.1×10^{-4} emu mol^{-1}). Because these compounds are metallic conductors, it is not surprising that they are essentially Pauli-paramagnetic. Pauli-paramagnetism originates from the itinerant conduction electrons associated with wide bands (*27, 28*). The values found for $TaPtTe_5$ and $NbPdTe_5$ are typical of those expected for Pauli-paramagnetism,

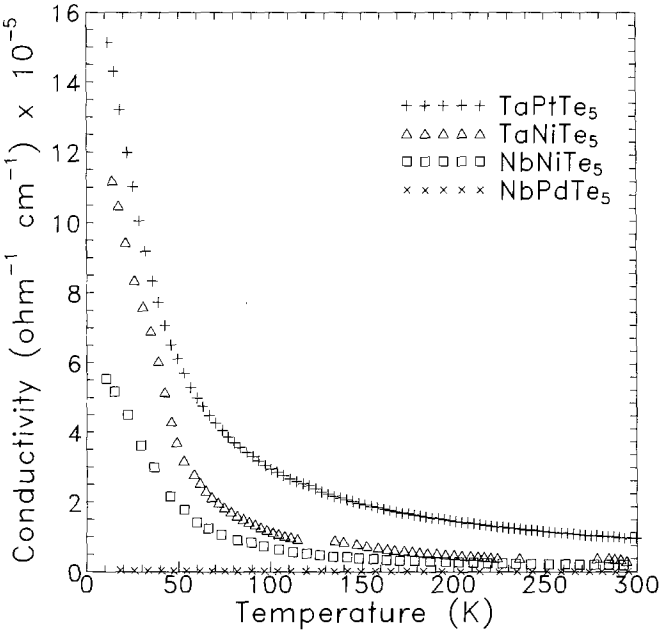

FIG. 4. Plots of electrical conductivity vs temperature along the needle axes a for single crystals of $TaPtTe_5$, $TaNiTe_5$, and $NbNiTe_5$, and along the needle axis b for $NbPdTe_5$. For $TaPtTe_5$, $\sigma_{298} = 9.7 \times 10^4\ \Omega^{-1}cm^{-1}$ and $\sigma_{10} = 1.5 \times 10^6\ \Omega^{-1}cm^{-1}$.

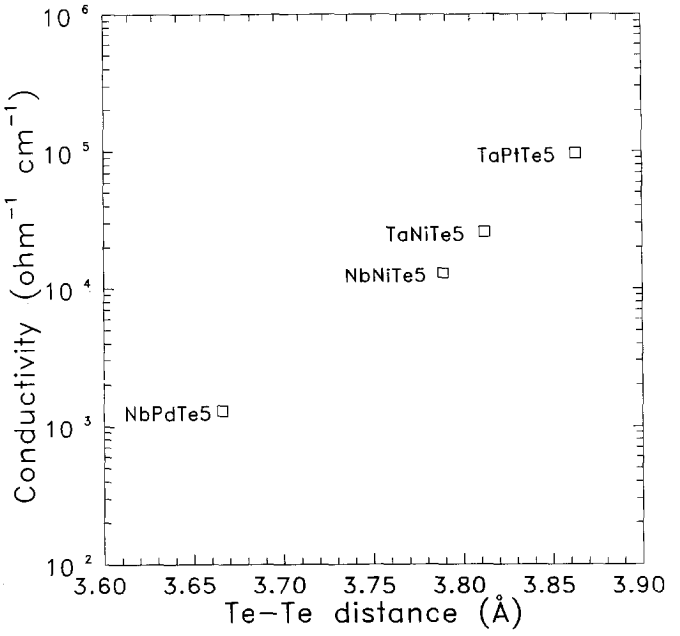

FIG. 5. Dependence of room-temperature electrical conductivity on shortest interlayer Te–Te distances for $TaPtTe_5$, $TaNiTe_5$, $NbNiTe_5$, and $NbPdTe_5$.

bearing in mind that even after correction for ion-core (or Larmor) diamagnetism, there may still be additional contributions from Landau diamagnetism and Van Vleck paramagnetism to a measured temperature-independent susceptibility (*29*): $\chi = \chi_{diam} + \chi_{Pauli} + \chi_{Landau} + \chi_{VV}$.

$NbNiTe_5$ and $TaNiTe_5$ display strongly temperature-dependent paramagnetism and their susceptibilities were fit by a least-squares procedure to the Curie–Weiss expression $\chi = (C/(T + \theta)) + \chi_o$, where C is the Curie constant, θ is the Weiss constant, and χ_o is a temperature-independent contribution. The values obtained are: C= 0.211(9), θ = 3.8(4), $\chi_o = 1.7(2) \times 10^{-3}$ for $NbNiTe_5$; C = 0.096(2) emu K mol^{-1}, θ = 3.3(2) K, χ_o = 1.3(1) 10^{-3} emu mol^{-1} for $TaNiTe_5$. An effective magnetic moment calculated from the formula (*30*) $\mu_{eff} = (8C)^{1/2}$, gives 1.30(3) and 0.88(1) μ_B for $NbNiTe_5$ and $TaNiTe_5$, respectively. (For one unpaired electron, a magnetic moment of 1.73 μ_B is expected.) The magnetic parameters obtained here are roughly comparable to those obtained previously (*13, 15*). The most likely impurities in these compounds are $NbTe_4$ or $TaTe_4$, which are diamagnetic (*31, 32*). We suspect that the presence of these impurities at levels undetectable by X-ray powder diffraction methods is responsible for the differences in χ_o. A strong correlation between C and θ was apparent in the least-squares analysis; this suggests that the Curie–Weiss expression is not an entirely appropriate model. Nevertheless, the temperature-dependent magnetic behavior of $NbNiTe_5$ and $TaNiTe_5$ is confirmed.

It is unusual for metallic compounds, such as $NbNiTe_5$ and $TaNiTe_5$, to exhibit temperature-dependent susceptibilities. But examples are known among other transition-metal chalcogenide systems (*29, 33*), for ex-

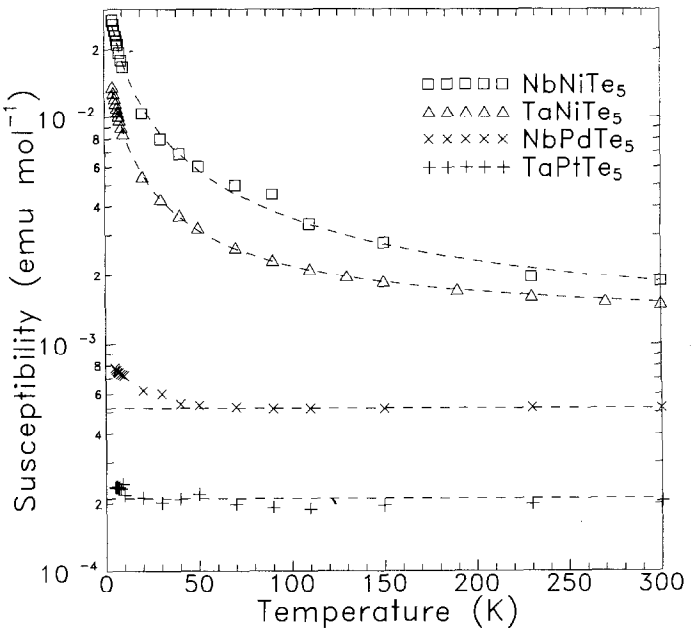

FIG. 6. Plots of molar magnetic susceptibility vs temperature for $NbNiTe_5$, $TaNiTe_5$, $NbPdTe_5$, and $TaPtTe_5$ at 5 kG. For $NbNiTe_5$ and $TaNiTe_5$, the dotted lines result from fits to the Curie–Weiss expression.

ample in some niobium and tantalum dichalcogenides intercalated with first-row transition metals (*30, 34–36*). The reasonable fit of the susceptibility data to the Curie–Weiss expression for $NbNiTe_5$ and $TaNiTe_5$ suggests that there may be some degree of localization of electrons associated with narrow bands, some of which are seen to be near the Fermi level in the calculated electronic structure of $NbNiTe_5$ (*25*). Substitution of Ni with the larger Pd and Pt atoms may disperse these narrow bands sufficiently to destroy this localized character and cause $NbPdTe_5$ and $TaPtTe_5$ to display their normal Pauli-paramagnetic behavior. Thus, in contrast to our earlier explanation of the trend in electrical conductivities, here we must invoke the role of the metal (Ni, Pd, Pt) as the overriding factor to account for the magnetic behavior of this series of compounds.

Clearly it would be desirable to synthesize the missing members of this series of compounds. Unfortunately, $TaPdTe_5$ and $NbPtTe_5$ remain elusive. In the Ta/Pd/Te system, the known phases are $Ta_3Pd_3Te_{14}$ (*15*) and $Ta_4Pd_3Te_{16}$ (*26*); in the Nb/Pt/Te system, no ternary phase has yet been isolated.

Acknowledgments

This research was supported by the U.S. National Science Foundation through Grant DMR-88-09854 (Science and Technology Center for Superconductivity) and Grant DMR-88-13623. Use was made of the SEM, electrical conductivity, and magnetic susceptibility facilities of the Materials Research Center at Northwestern University (U.S. National Science Foundation Grant DMR-88-21571). We thank Johnson Matthey Ltd. for loan of the Pt powder.

References

1. W. W. FULLER AND P. M. CHALKIN, *Solid State Commun.* **30,** 689 (1979).
2. F. R. GAMBLE, F. J. DISALVO, R. A. KLEMM, AND T. H. GEBALLE, *Science* **168,** 568 (1970).

3. M. H. VAN MAAREN AND H. B. HARLAND, *Phys. Lett. A* **29,** 571 (1969).
4. M. H. VAN MAAREN AND G. M. SCHAEFFER, *Phys. Lett. A* **24,** 645 (1967).
5. F. W. BOSWELL, A. PRODAN, AND J. K. BRANDON, *J. Phys. C* **16,** 1067 (1983).
6. J. A. WILSON, *Phys. Rev. B* **19,** 6456 (1979).
7. D. E. MONCTON, J. D. AXE, AND F. J. DISALVO, *Phys. Rev. B* **16,** 801 (1977).
8. F. J. DISALVO AND T. M. RICE, *Physics Today* **32,** 32 (Apr. 1979).
9. F. LÉVY (Ed.), "Crystallography and Crystal Chemistry of Materials with Layered Structures, Vol. 2, Physics and Chemistry of Materials with Layered Structures," Reidel, Dordrecht (1976).
10. A. J. JACOBSON, *in* "Intercalation Chemistry" (M. S. Whittingham and A. J. Jacobson, Eds.), p. 229, Academic Press, New York (1982).
11. A. D. YOFFE, *Ann. Chim. Fr.* **7,** 215 (1982).
12. S. A. SUNSHINE, D. A. KESZLER, AND J. A. IBERS, *Acc. Chem. Res.* **20,** 395 (1987).
13. E.W. LIIMATTA AND J. A. IBERS, *J. Solid State Chem.* **71,** 384 (1987).
14. E. W. LIIMATTA AND J. A. IBERS, *J. Solid State Chem.* **77,** 141 (1988).
15. E. W. LIIMATTA AND J. A. IBERS, *J. Solid State Chem.* **78,** 7 (1989).
16. T. E. PHILLIPS, J. R. ANDERSON, C. J. SCHRAMM, AND B. M. HOFFMAN, *Rev. Sci. Instrum.* **50**(2), 263 (1979).
17. L. N. MULAY AND E. A. BOUDREAUX, Eds., "Theory and Application of Molecular Diamagnetism," Wiley–Interscience, New York (1976).
18. J. M. WATERS AND J. A. IBERS, *Inorg. Chem.* **16,** 3273 (1977).
19. D. T. CROMER AND J. T. WABER, "International Tables for X-Ray Crystallography," Vol. IV., Table 2.2A; D. T. Cromer, Table 2.3.1, Kynoch Press, Birmingham, England (1974).
20. R. D. SHANNON, *Acta Crystallogr. Sect. A* **32,** 751 (1976).
21. P. M. KEANE AND J. A. IBERS, *Inorg. Chem.* **30,** 1327 (1991).
22. P. M. KEANE AND J. A. IBERS, *Inorg. Chem.*, in press.
23. S. FURUSETH, L. BRATTÅS, AND A. KJEKSHUS, *Acta Chem. Scand.* **27,** 2367 (1972).
24. P. BÖTTCHER, *Angew. Chem. Int. Ed. Engl.* **27,** 759 (1988).
25. J.-F. HALET, R. HOFFMANN, W. TREMEL, E. W. LIIMATTA, AND J. A. IBERS, *Chem. Mater.* **1,** 451 (1989).
26. A. MAR AND J. A. IBERS, *J. Chem. Soc. Dalton Trans.*, in press.
27. C. KITTEL, "Introduction to Solid State Physics," 6th ed., Wiley New York (1986).
28. N. W. ASHCROFT AND N. D. MERMIN, "Solid State Physics," Saunders, Philadelphia (1976).
29. J. M. VANDENBERG-VOORHOEVE, *in* "Optical and Electrical Properties, Vol. 4, Physics and Chemistry of Materials with Layered Structures," (P. A. Lee, Ed.), p. 423, Reidel, Dordrecht (1976).
30. J. M. VAN DEN BERG AND P. COSSEE, *Inorg. Chim. Acta* **2,** 143 (1968).
31. K. SELTE AND A. KJEKSHUS, *Acta Chem. Scand.* **19,** 258 (1965).
32. F. HULLIGER, *Struct. Bonding* **4,** 83 (1968).
33. A. B. DE VRIES AND C. HAAS, *J. Phys. Chem. Solids* **34,** 651 (1973).
34. K. ANZENHOFER, J. M. VAN DEN BERG, P.COSSEE, AND J. N. HELLE, *J. Phys. Chem. Solids* **31,** 1057 (1970).
35. F. HULLIGER AND E. POBITSCHKA, *J. Solid State Chem.* **1,** 117 (1970).
36. A. MEERSCHAUT, M. SPIESSER, J. ROUXEL, AND O. GOROCHOV, *J. Solid State Chem.* **31,** 31 (1980).
37. J. C. HUFFMAN, Ph.D. thesis, Indiana University (1974).
38. J. DE MEULENAER AND H. TOMPA, *Acta Crystallogr.* **19,** 1014 (1965).
39. P. G. LENHERT, *J. Appl. Crystallogr.* **8,** 568 (1975).